이학석사 학위논문

Magnetic proximity effect between $NbSe_2$ and $CrPS_4$ Van der Waals heterostructure

반강자성체 $CrPS_4$와 초전도체 $NbSe_2$ 반데르발스 이종접합 구조에서의 자기 근접 효과

2020년 8월

서울대학교 대학원
Seoul National University
물리・천문학부
신 제 철

Master’ s Thesis of Natural Science

Magnetic proximity effect between $NbSe_2$ and $CrPS_4$ Van der Waals heterostructure

August 2020

Graduate School of Natural Science
Seoul National University
Department of Physics and Astronomy

Jea Cheol Shin

Abstract

In the junction of superconductor (SC) and ferromagnet (FM), the superconductivity can be tuned by exchange fields originating from FM. In the FM/SC/FM structure, using the phenomenon that the stronger the exchange field, the weaker the superconductivity, the control of superconducting transition temperature (T_C) and infinite magnetoresistance (MR) according to the relative magnetization orientation between the two FM layers were reported. Furthermore, recently, the separation of Bardeen–Cooper–Schrieffer (BCS) singularity in the EuS/Al structure was also realized even in no external magnetic field. Previous research, however, are lack of studies in various systems, and have not been carried out on the single crystalline 2D van der Waals (vdW) materials. Taking advantage of this cleanness of 2D materials, we performed our research using vdW SC $NbSe_2$ and antiferromagnetic insulator (AFI) $CrPS_4$. In $CrPS_4$/$NbSe_2$/$CrPS_4$ structure, it was confirmed that the superconducting state of the $NbSe_2$ layer could be broken by the exchange field of $CrPS_4$, and the region of non–dissipative transport could be varied according to the relative magnetization of two $CrPS_4$ layers, producing Infinite MR. However, because some results such as separation of BCS singularity and suspected spin transport were

not confirmed due to the structural problems of our devices, further experiments are currently being planned by designing new devices. Nevertheless, through the fact that clear magnetic proximity effects between $NbSe_2$ and $CrPS_4$ were identified for the first time in an vdW heterostructure, we suggest that the $CrPS_4/NbSe_2$ heterostructure can be a new and potential platform for studying exchange field between SC and FM.

Keywords: 2D superconductor, 2D antiferromagnetic insulator, van der Waals heterostructure, Electric transport measurement, Niobium diselenide, Chromium thiophosphate.

Student Number: 2018-28679

Table of Contents

List of Figures

Chapter 1. Introduction

1.1. Motivation and Outline of Research

The proximity effects between ferromagnet (FM) and superconductor (SC) have been intensively studied since superconducting properties can be manipulated by exchange field of FM penetrating into the depth comparable to superconducting coherence length[1,2]. Through the phenomenon that the superconductivity is weakened by exchange field, in the FMM/SC/FMM structure, where FMM is ferromagnetic metal, various studies have confirmed that superconducting transition temperature (T_C) can be controlled through the relative magnetization of two FM layers[3-6]. Also, recently, ferromagnetic insulator (FI) in contact with SC is under study to exclude the complicate interaction between FMM and SC such as spin injection. In this ideal system with FI and SC, it was revealed that infinite magnetoresistance (MR) in FI/SC/FI[7,8] and separation of Bardeen-Cooper-Schrieffer (BCS) singularity for the spins can be produced in FI/SC structure[2,9-11], bringing great advance to the superconducting spintronics[12].

Previous research, however, are lack of studies in various systems, and have not been carried out on the 2D van der Waals (vdW) materials. Although the vdW materials have the advantage of being able to fabricate heterostructure device in defectless single-crystalline regime with clean interfaces through exfoliation technique[13–15], representative 2D SCs[16–22] like MoS_2 and $NbSe_2$ have low yield of fabrication, and previously studied 2D magnetic materials are normally metallic or air-sensitive[23,24], limiting fabrication of ideal FI/SC vdW heterostructure.

Here, using novel dry transfer techniques with polycaprolactone (PCL) developed in professor Je-Geun Park's lab from Seoul National University, we fabricate $CrPS_4/NbSe_2/CrPS_4$ structure that could not be made in the conventional way, whereby $CrPS_4$ is an air-stable 2D antiferromagnetic insulator (AFI)[25]. For our ideal AFI/SC/AFI sandwiched structure, it was confirmed that the superconductivity could be broken by the exchange field of $CrPS_4$, and the infinite MR, produced by the relative orientation of the magnetization of two $CrPS_4$ layers, was generated for the first time in a 2D vdW heterostructure.

However, analyzing the presence of exchange splitting and other curious results, which might be caused by spin transport, was in trouble because of several faults in the current device structure.

Thus, for an accurate verification of these effects, further experiments are currently being planned, starting with a revision of the device structure.

Chapter 2. Experimental Background

2.1. Tuning Superconductivity by Controlling Internal Exchange Fields and Infinite Magnetoresistance

In the FM/SC/FM structure, superconductivity depends on the relative configuration of the magnetization between the two FM layers. If the magnetization of the upper and lower FM layers has a parallel configuration, the internal exchange fields become strong as the same direction of effective fields is applied to the SC layer. However, if the magnetization of the two FM layers exhibits anti-parallel ordering, the exchange fields felt by the superconducting layer are canceled and relatively weak fields are applied. This control of the relative orientation of magnetization can be performed through adjusting the thickness of the two FM layers in order to vary coercivity. For this tri-layered structure, studies had been actively carried out to control the superconducting transition temperature (T_C)[3–6] by varying the configuration of the magnetization between the two FM layers. Moreover, it has been experimentally confirmed that even an infinite MR can be produced[7,8] .

The mechanism of infinite MR is shown in Figures 2.1 and 2.2. In high fields, in which the magnetization of the two FM layers is parallel, the exchange field felt by the SC layer is strong, resulting in a finite resistance with broken superconductivity. Sweeping the magnetic field in the opposite direction causes the FM layer with lower coercivity to switch first; this causes the magnetization of the two FM layers to be anti-parallel, resulting in a zero-resistance state. This clean and dramatic change indicates that the FM/SC/FM system has a strong potential for use in logic circuits and memory devices with an extremely low error rate[12].

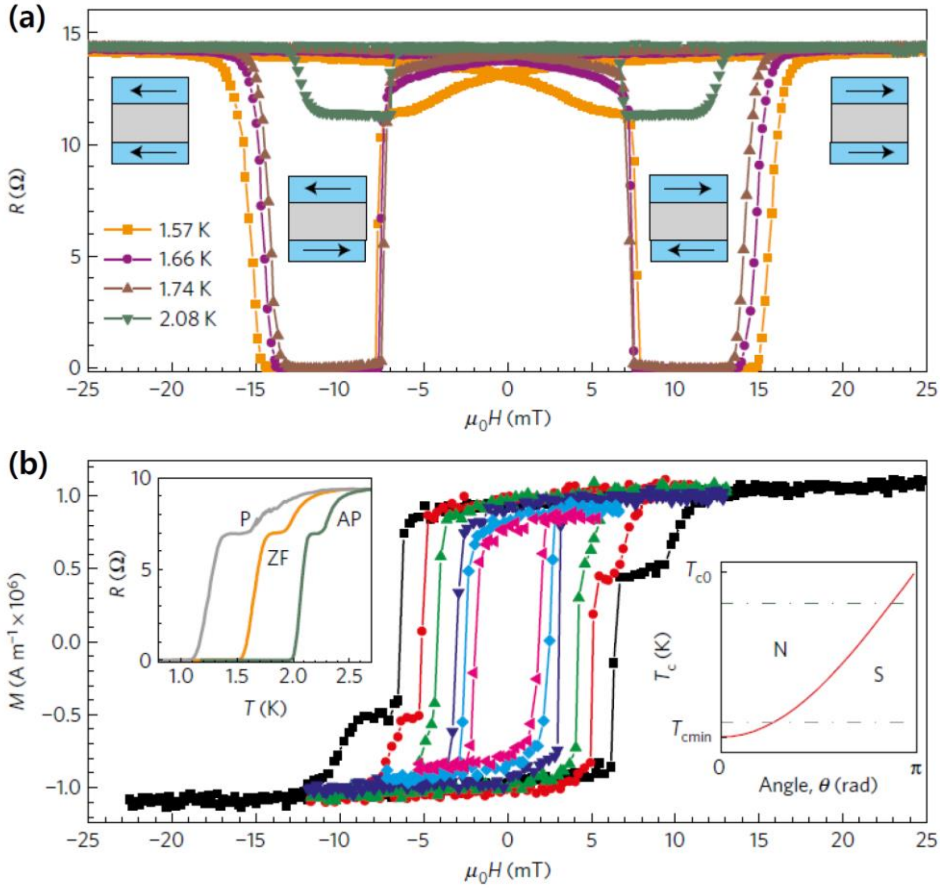

Figure 2.1 Infinite magnetoresistance in a GdN(3)/Nb(8)/GdN(5) device (thickness in nm)[8] (a) Resistance as a function of external magnetic field. (b) Magnetic hysteresis loop of the two GdN layers.

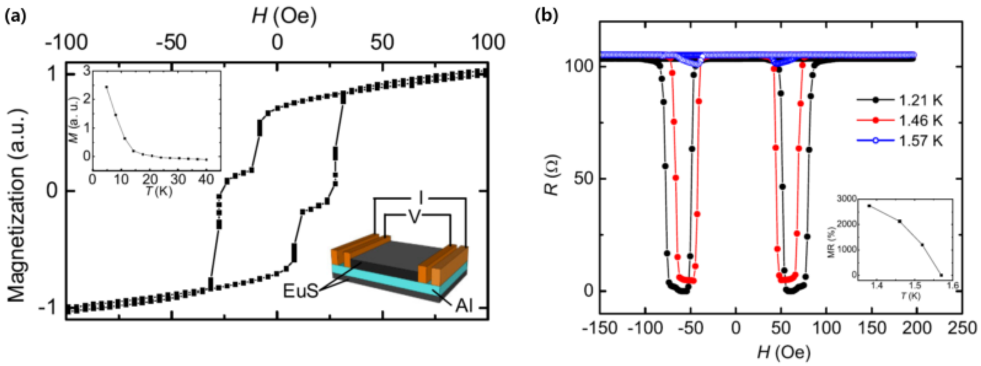

Figure 2.2 Infinite magnetoresistance in a EuS(1.5)/Al(3.5)/EuS(4) device (thickness in nm)[7] (a) Magnetic hysteresis loop of the two EuS layers. (b) Infinite magnetoresistance of the device.

2.2. Separation of BCS Singularity Induced by Exchange Field

The separation of a BCS singularity near the superconducting gap is regarded as an experimental platform for studying Majorana bound states[12,26]. As depicted in Figure 2.3, a BCS singularity N(E) for spins can be separated by Zeeman splitting. However, Zeeman splitting requires strong magnetic fields, because of the weak magnitude of the splitting, $2\mu_B H$, calculated to be ~115 μeV/T[12,27,28]. Fortunately, recent studies have revealed that this strong magnetic field can be substituted by joining SC with FI[2,9–11]. In the FI/SC structure, the SC layer feels an exchange field in the range of several T into a depth comparable with the superconducting coherence length[1,2]. Thanks to these strong exchange fields, a splitting of the BCS singularity can be induced even for a small range of external magnetic fields, called exchange splitting.

Figure 2.4 shows previous research observing the separation of the BCS singularity in an EuS/Al structure through differential tunneling conductance[2]. As shown in Figure 2.4 (c), the splitting is enhanced when the magnetization of the FI (EuS) layer is fully polarized. As sweeping the external magnetic fields (Figure 2.4 (b)), the splitting is weakened and then enhanced again at the coercive field of the EuS layer, indicating that the splitting is originated from the magnetization of EuS, not from the Zeeman effect. The magnitude of the exchange splitting ($2\hbar_{ex}$) evolves from 110 μeV to 190 μeV, depending on magnetization, and corresponding to the magnitude of the exchange field $B_{ex} = \frac{\hbar_{ex}}{g\mu_B} \approx 1 \sim 1.6$ T, where $g \approx 2$ is the Landé g−factor, and μ_B is the Bohr magneton.

2.3. Significance of Our Research

As mentioned above, there are several obvious effects originating from exchange fields, such as infinite MR and exchange splitting for a small range of fields. However, there are few studies on the various systems. In addition, controlling cleanness of the interfaces and crystal qualities for the materials, which are decisive for investigating exchange fields between SCs and FMs, is quite a challenging issue in polycrystalline nanofilms. These problems, however, are not matter for vdW heterostructure because it provides clean interfaces and single−crystalline materials for each layer. Therefore, vdW heterostructures have a strong potential to be a new platform for investigating exchange fields between SCs and FMs.

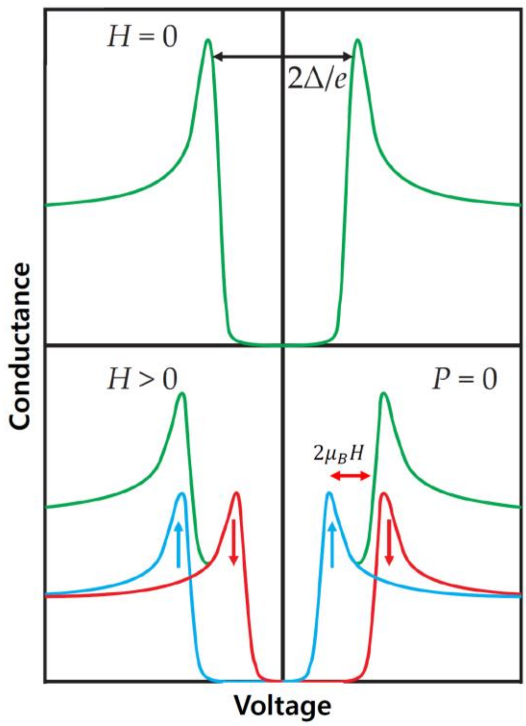

Figure 2.3 Separation of BCS singularity for spins due to Zeeman splitting[27].

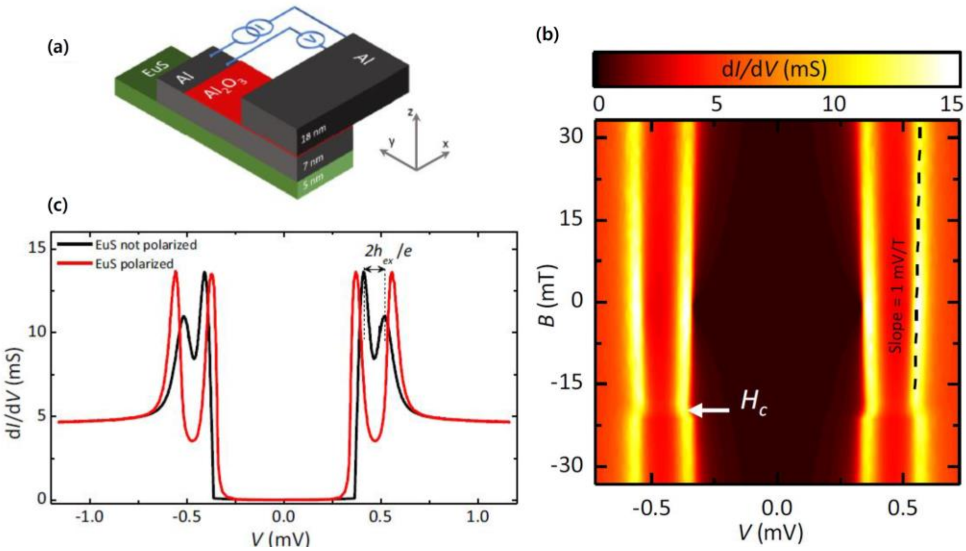

Figure 2.4 Exchange splitting in EuS/Al bilayer[2]. (a) Schematic of the EuS/Al/Al_2O_3/Al vertical tunnel junction. (b) Evolution of the magnitude of splitting by sweeping external in−plane magnetic field. (c) Comparison of differential conductance between EuS unpolarized (black trace) and polarized (red trace) states at zero magnetic fields.

Chapter 3. Method

3.1. Device Fabrication

All devices were fabricated by Su-Han Son, from professor Je-Geun Park's lab, Seoul National University.

Three different $CrPS_4/NbSe_2/CrPS_4$ devices (see Figure 3.1) were fabricated using a polycaprolactone (PCL) stamp. For the preparation of the PCL stamp, PCL was dissolved in a tetrahydrofuran (THF) solvent, and then spin-coated on a transparent tape attached to a PDMS block.

Pick-up and drop-down were made using the following procedures. First, the PCL stamp was moved down to the target flake on the substrate at 55 ℃. By increasing the temperature to 65 ℃, the PCL film was melted to fully enclose the flake. Next, after cooling the film to 30 ℃, a micro-manipulator was slowly retracted to pick up the flake. These procedures were repeated for a continuous pick-up of the vdW heterostructure. In the final step of drop-down, the PCL stamp was moved close to the pre-patterned Pt(18 nm)/Ti(2 nm) electrodes followed by completely melting the PCL film at 75 ℃.

The micro−manipulator was then slowly retracted to isolate the PCL stamp from the substrate. After drop−down, PCL residue on the substrate was removed by keeping the devices in THF solvent overnight.

Considering a vertical superconducting coherence length of $NbSe_2$ (~6.9 nm at 1.6 K)[29,30], the thickness of the $NbSe_2$ flakes was controlled to within less than 10 nm, so that all area of the $NbSe_2$ to be affected by exchange field of top or bottom $CrPS_4$ layers. In the case of $CrPS_4$, the thickness of the two layers was adjusted differently to vary the coercive field of each layer.

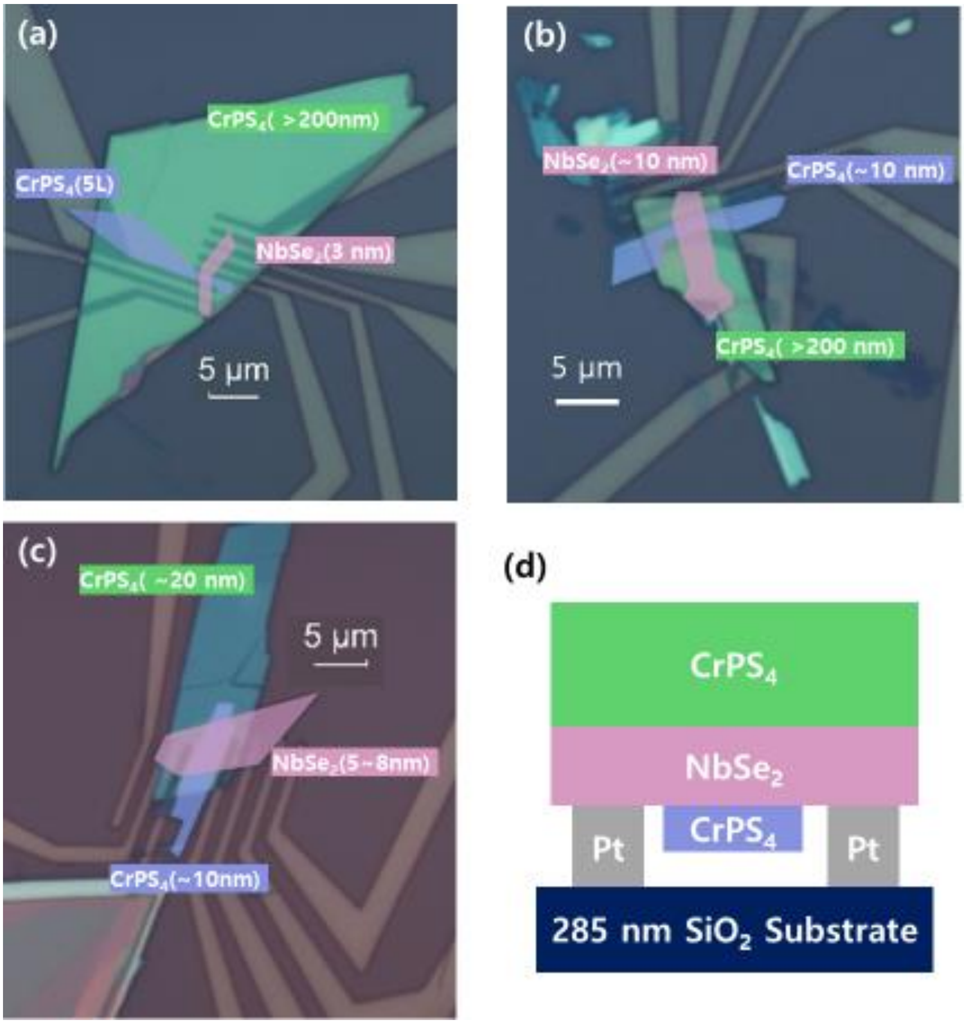

Figure 3.1 Optical images of $CrPS_4/NbSe_2/CrPS_4$ devices. Thickness information is depicted inside. (a) sample A, (b) sample B, (c) sample C, (d) Schematic side view of the devices.

3.2. Electronic Transport Measurement

The 2−terminal differential conductance was measured using the lock−in technique. Considering the large resistances of the electrodes themselves (~kΩ), a small AC excitation of δV_{AC}=300 ~ 500 μV was mixed with DC bias voltage using a high quality audio transformer (VTX−101−006, Vigortronix). Alternating (differential) and direct current signals were recorded simultaneously using a lock−in amplifier (Model 7265, Signal Recovery) and DC voltmeter (Model 2182, Keithley Instruments) connected to a current preamplifier (Model 1211, DL instrument). For the 4−terminal voltage−current characteristics, direct voltage and a current source (Model 7651, Yokogawa Corporation) and DC voltmeter (Model 2182, Keithley Instruments) were used. The temperature and magnetic fields were controlled using a ^{4}He integrated superconducting magnet system (Teslatron PT, Oxford Instruments) with a base temperature of 1.54 K (stability of ± 5 mK) and maximum magnetic field of 8 T.

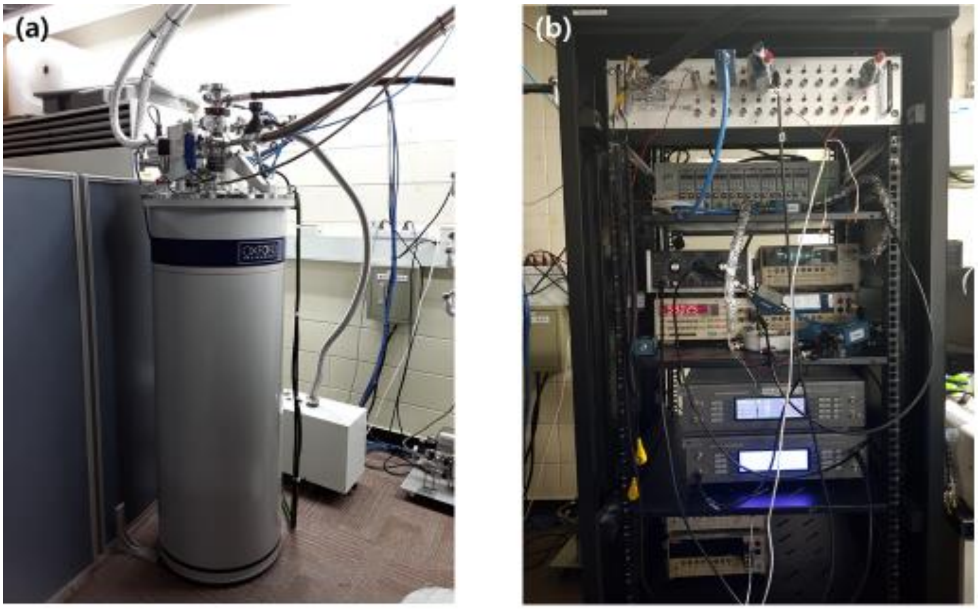

Figure 3.2 (a) Oxford Teslatron PT (b) Measurement setup for lateral magneto−transport measurements

Chapter 4. Lateral Electronic Transport Properties of $CrPS_4$ and $NbSe_2$ Heterostructure

4.1. Pre-summary

Lateral electronic transport properties of three different $CrPS_4/NbSe_2/CrPS_4$ devices were investigated at 1.54 K. The magnetization of $CrPS_4$ layers, which has a perpendicular magnetic anisotropy[24,25,31], was controlled by applying a perpendicular magnetic field of maximum 8 T.

4.2. Effect of Exchange Field on Superconducting $NbSe_2$

Effects of exchange fields between $CrPS_4$ and $NbSe_2$ of sample A and sample C were investigated through temperature-resistance and voltage-current ($V-I$) characteristics.

As shown in Figure 4.1 (a) and indicated by the blue trace in Figure 4.1 (c), in the region of the sandwiched $NbSe_2$ of sample A, the resistance did not fall to zero below T_C and non-dissipative transport was not visible in the $V-I$ characteristics, thereby implying a strong exchange field in the sandwiched region. In sample C (Figure 4.1(b), (c)), however, superconductivity was detected in the same sandwiched $NbSe_2$ region. This difference, presence or absence of non-dissipative transport in the same sandwiched region, can be explained by the magnetic ordering of $CrPS_4$[24,25,31] and the vertical coherence length of $NbSe_2$[29,30]. Because the magnetic ordering of the $CrPS_4$ nanofilm has opposite spin directions for alternate layers such as CrI_3[24,25,31,32], for a few layers of $CrPS_4$, the odd-layered film has a stronger magnetization than the even-layered one. Based on a previous study of the FM1/FM2/SC structure showing T_C dependence according to the relative orientation of the magnetization of two FM layers[33], it is reasonable to assume that the 5-layered $CrPS_4$ in sample A exhibits a stronger exchange field than a sample with dozens of layers. In addition, $NbSe_2$ in sample A was 3 nm thick, which is thinner than the vertical superconducting coherence length of $NbSe_2$ at 1.6 K(~6.9 nm)[29,30] — i.e., the average exchange field experienced by the sandwiched region of sample A could be strong enough to induce the pair breaking effect.

Therefore, the thickness of the vdW flake needs to be adjusted more precisely for further experiments. For $NbSe_2$, it should not be too much thinner than the vertical superconducting coherence length. The thickness of $CrPS_4$ seemed more crucial, because of its layer by layer antiferromagnetic ordering resulting in a stronger magnetization in samples with an odd number of layers. Hence, the number of $CrPS_4$ layers should be exactly counted, so that a comparison of magnitudes of exchange fields between odd and even layered samples can be carried out.

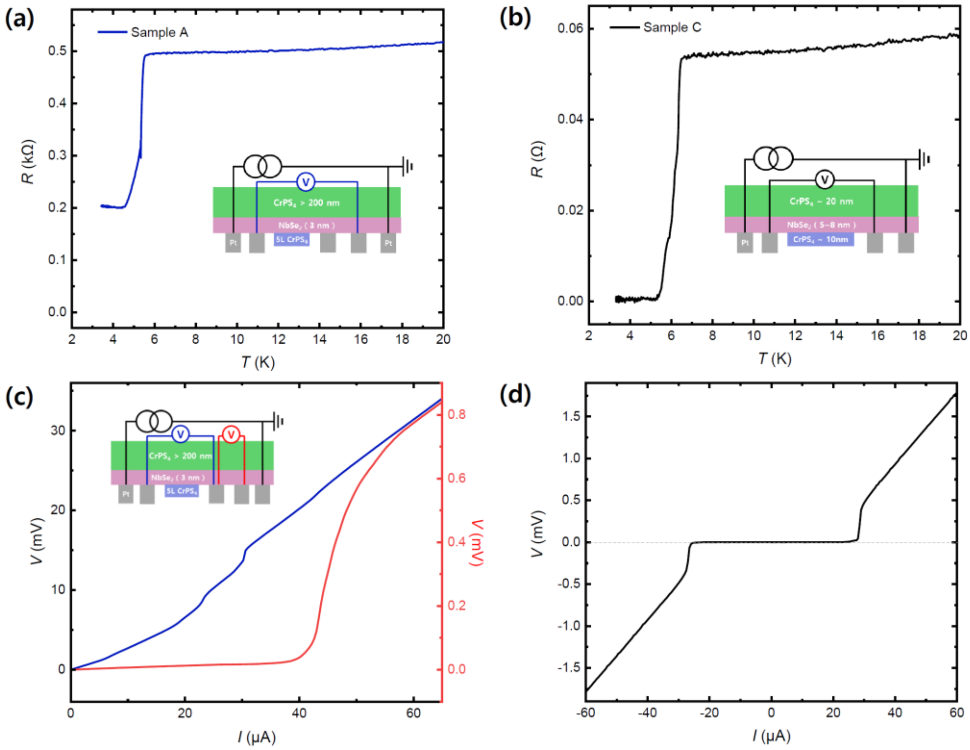

Figure 4.1 Effect of exchange field on superconductivity of $NbSe_2$. Geometry of measurement is depicted inside. (a), (b) Temperature–resistance characteristics of sample A and sample C, respectively. (c), (d) V–I characteristics of sample A and sample C, respectively.

4.3. Infinite Magnetoresistance Controlled by Magnetic Ordering between Top and Bottom $CrPS_4$

The superconducting state of the $NbSe_2$ film in sample C was controlled by adjusting H for tuning the internal exchange field.

The variations in the superconducting state according to the magnetic configuration of two $CrPS_4$ are shown in Figure 4.2. As the thickness of the two $CrPS_4$ layers were adjusted differently, the relative configuration of the magnetization, parallel or anti−parallel orientation, could be controlled by sweeping H. As shown in Figure 4.2 (a), for an anti−parallel ordering of the magnetization, the internal exchange field felt by $NbSe_2$ became smaller, increasing the critical current (I_C). As H was reversed, $CrPS_4$ layer having a smaller coercive field switched first to produce a parallel configuration, enhancing the exchange field felt by $NbSe_2$ and reducing I_C − i.e., the black regions in which non−dissipative transport exists shrink and widen with the sweeping of H. Using these variations of I_C, infinite MR can be generated. Figures 4.2 (b) and (c) are the 25 μA cross−section of Figure 4.2 (a) and the results of direct measurements when sweeping H with the DC current fixed at 25 μA, respectively. Both results show hysteresis behavior depending on the sweep direction of H, which is evidence that the exchange field felt by $NbSe_2$ can be tuned by the magnetic configuration of the two $CrPS_4$ layers, parallel or anti−parallel. The reason for the several observed dips in resistance, which are different from previous studies showing only one sharp dip at a single sweep of H [7,8], is the antiferromagnetic ordering of $CrPS_4$ going through multiple switching, similar to case in CrI_3[24,25,32,34]. Our results also show that the fields needed to flip the magnetization of a single layer of $CrPS_4$ is in the order of a few to a few tens of mT, which was not previously reported.

However, resistance dips in our sample were a lot messier than those observed in previous studies[7,8], which might have been caused by the complicated magnetic ordering of dozens of layers $CrPS_4$, and also some faults in the structure of the devices resulting in I_C being unstable in the finite magnetic fields, which are described in Chapter 4.5.

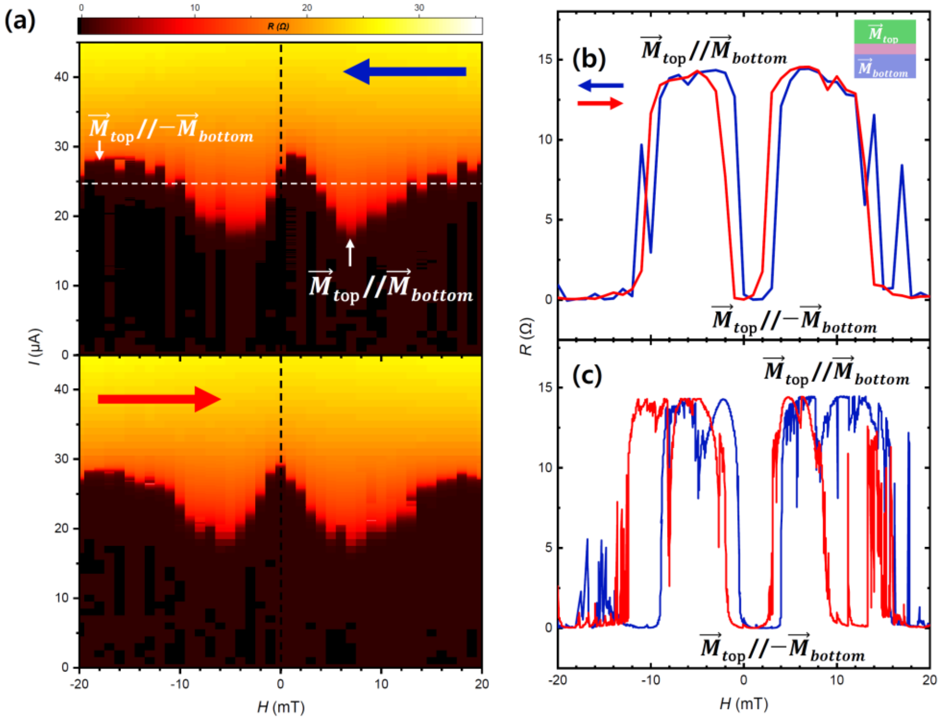

Figure 4.2 Infinite magnetoresistance of sample C. Sweep directions of external magnetic fields were marked by blue and red arrows. (a) Current−R_{DC} characteristics as a function of H. DC current was swept from positive to negative. (b) 25 μA cross−section of (a). (c) Directly measured $R_{DC}(H)$ when sweeping H. 25 μA of DC current was biased.

Shown in Figure 4.3, numerous shrinking and widening events of the non-dissipative transport regions were observed because dozens of layers of $CrPS_4$ produce a lot of switching. Remarkably, as shown in Figure 4.3(a), the region of non-dissipative transport (black region) shows nearly symmetric patterns with respect to the origin (I=H=0). However, considering slightly misaligned symmetric point from the origin and the V−I traces at 0 T (see Figure 4.3(b)) are shifted differently according to the sweep direction of H, this unexpected pattern seems to originate from the magnetization of $CrPS_4$, not from external magnetic fields as in the self-field effect in a Josephson junction[35]. Based on this speculation, we suspected spin transport in the $NbSe_2$ film affected by magnetization could exist. But as explained before, numerous switches in magnetization, which produce uncountable configurations of magnetic ordering, and unstable I_C under finite magnetic fields make the analysis too complicated. In addition, suspected spin transport could have several possible origins, such as spin injections from Pt due to the spin Hall effect[36–40] or the normal states of $NbSe_2$ having spin−valley locking[41–45]. To generate a simpler and more ideal system, it was necessary to replace Pt in the electrodes with Au.

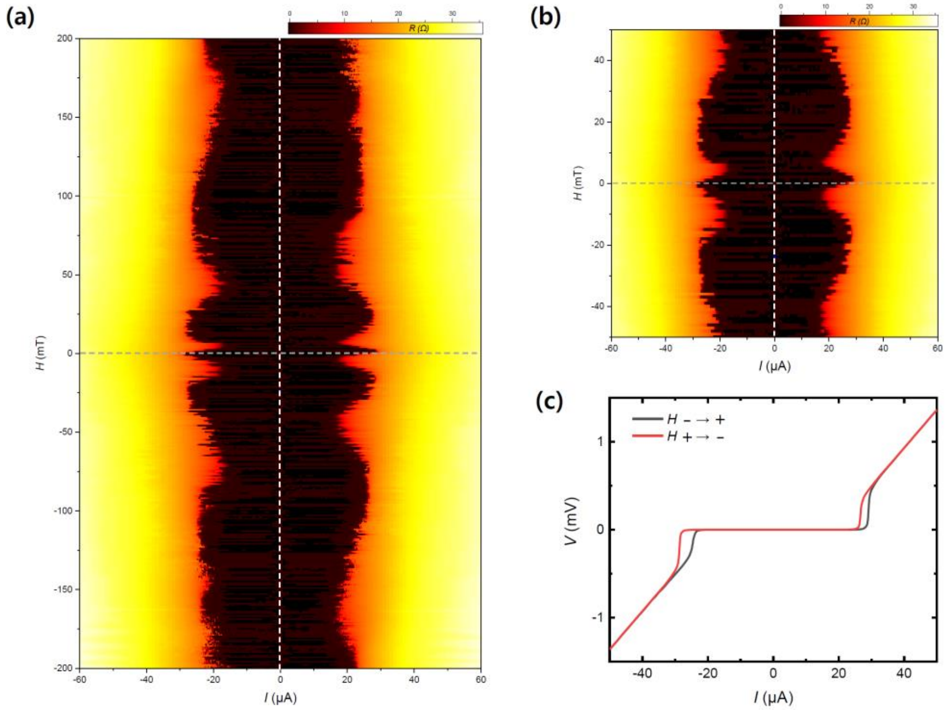

Figure 4.3 Current−voltage characteristics of sample C (a), (b) I−R_{DC} as a function of H. Positive to negative sweep of I and H was performed. (b) V−I characteristics at 0 T according to sweep direction of H.

4.4. Direct Differential Conductance Measurement

Direct differential conductance measurements were performed to investigate a separation of the BCS singularity induced by the exchange field. Although some peaks, which might have been caused by the exchange splitting, were observed in sample B (see Figure 4.4 (a)), there were limitations on performing further analysis because the exact superconducting state could not be confirmed due to access to only three usable electrodes. Unlike for sample B, no other peaks were observed in sample C (Figures 4.4 (b), (c)), and investigation under finite magnetic fields could not be performed due to unstable I_C, which is consistent with the results shown in Figure 4.2.

Although clear evidence of the exchange splitting was not discovered, considering some peaks observed in sample B, which might indicate other energy states, there still exists the possibility of a detectable exchange splitting in the $CrPS_4/NbSe_2$ structure. To verify this, more accurate experiments are needed, for which a redesign of the device is necessary.

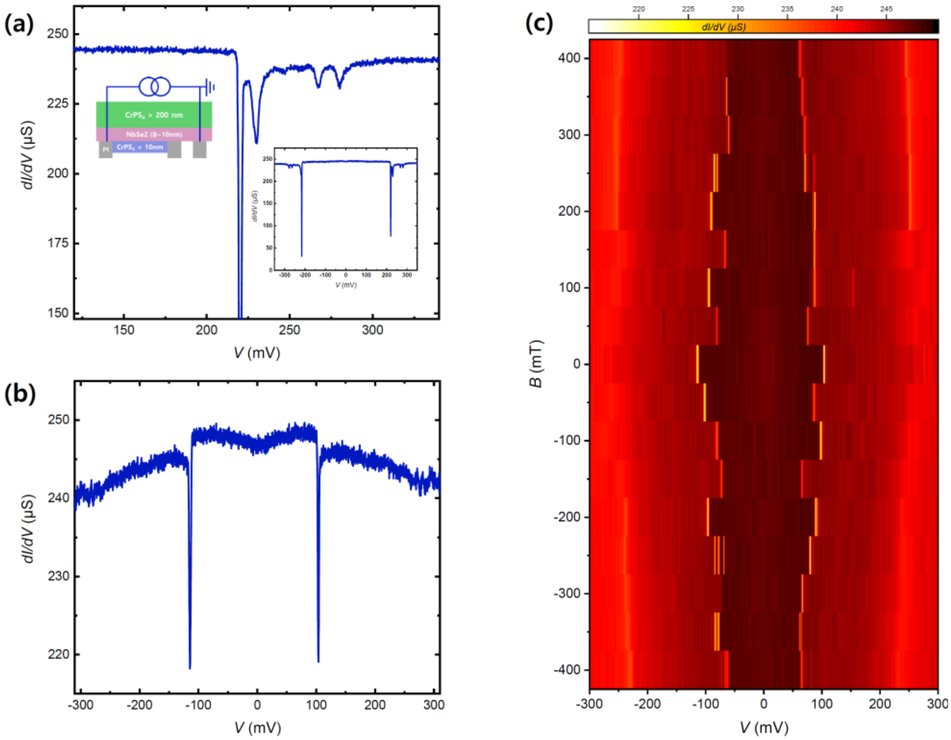

Figure 4.4 Differential conductance of sample B (a) and sample C (b) at 0 T. (c) *dI/dV* as a function of *H* of sample C.

4.5. Faults of the Current Device Structure and Revised Design for Further Experiments

As described in Chapter 4.3, although there was clear evidence that the exchange field felt by $NbSe_2$ depends on the magnetic configuration of the two $CrPS_4$ layers, there were constraints in performing a more accurate analysis because of the complicated ordering of $CrPS_4$ and difficulty with measurements, such as unstable I_C under finite magnetic fields. For further experiments and investigations, the drawbacks of the current device structure and possible mitigating modifications are mentioned below.

First, the electrodes themselves were problematic. As shown in Figure 4.5(a), the conductance of sample B showed significant differences depending on the set of electrodes used, meaning that the resistance of the electrodes (or the contact between electrodes and the device) differed from one another. In addition, dI/dV values of normal and superconducting states showed only ~2% of difference, indicating that the conductance of the electrodes themselves should be subtracted. Furthermore, to avoid the possibility of spin injection from Pt electrodes due to the spin Hall effect[36-40], as mentioned in Chapter 4.3, the Pt should be replaced by another and more suitable material.

Secondly, the structure of the devices caused faults. As shown in Figure 4.5 (b), an extrapolation of the linear resistance region does not pass through the origin ($I=V=0$). In other words, there existed excess currents; an extrapolation of a normal state passed through the origin only when the larger currents were biased (inset of Figure 4.5 (b)). Furthermore, the voltage signal near I_C was very unstable under finite magnetic fields (Figure 4.5 (c)), while not at 0 T. These issues were caused by the structure of the devices. Due to the current structure (Figure 4.6 (a)) of placing a vdW heterostructure on pre-patterned electrodes (20 nm-thick), there are areas in which the device experiences mechanical strain, which can create the nucleation of a phase slip line (PSL)[46-49]. These PSLs refer to the rivers of fast vortices and antivortices that are annihilated in the middle of the sample, and are observed through discontinuous voltage jumps, whereby an extrapolation of the current axis leads to finite excess currents. In previous research with a device structure similar to ours, where the $NbSe_2$ flake was mounted on a 17 nm thick electrodes, these series of voltage jumps and unstable I_C under finite magnetic fields were reported[49].

To eliminate these problems, we designed a new device (Figure 4.6 (b)). First, as mentioned in Chapter 4.3, it is necessary to analyze the $CrPS_4/NbSe_2$ bilayer structure by adjusting the layers of $CrPS_4$ to be countable. Second, the electrode structure needs to be modified, so that the resistance of the electrodes themselves can be measured and subtracted from the entire conductance. Additionally, the pre-patterned Pt electrodes should be replaced by Au deposited on the devices to avoid the possibility of spin injection from Pt without straining the $NbSe_2$ flake. In this revised design, as uncountable flipping of magnetization and unstable I_C under finite fields would be suppressed, it is expected that an analysis of exchange splitting and the origin of suspected spin transport will be possible by controlling the magnetization of $CrPS_4$, which could not be clearly identified in the current $CrPS_4/NbSe_2/CrPS_4$ structure.

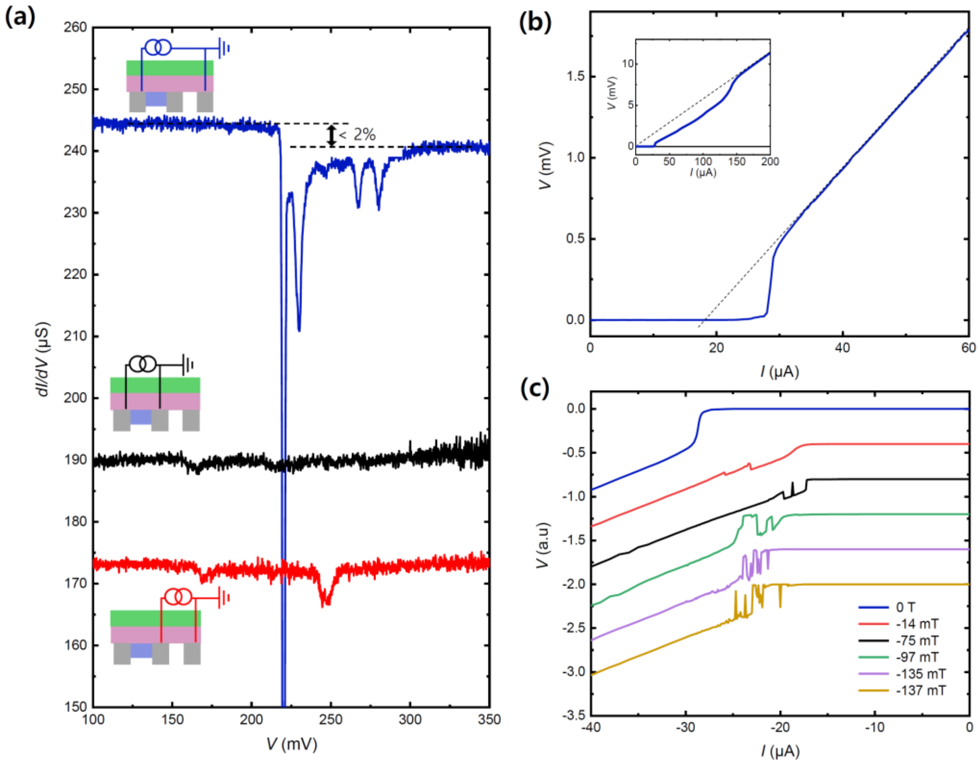

Figure 4.5 Electronic transport properties implying drawbacks of the devices. (a) Differential conductance of sample B according to set of electrodes used. (b), (c) $V-I$ characteristics of sample C at 0 T (b) and various magnetic fields (c).

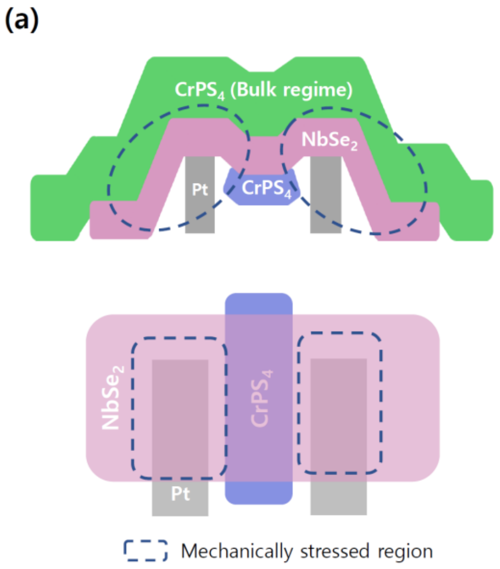

Figure 4.6 Schematics of current and revised devices. (a) Mechanically stressed region of current $CrPS_4/NbSe_2/CrPS_4$ devices. (b) Schematic design of revised device.

Chapter 5. Conclusion

As novel dry transfer technique using polycaprolactone (PCL) allows the fabrication of a new type of vdW heterostructure, proximity effects in the FM/SC structure were investigated in a vdW heterostructure in the clean single crystal regime using $NbSe_2$ and $CrPS_4$.

In the $CrPS_4/NbSe_2/CrPS_4$ structure, by confirming that the regions at which non-dissipative transport occurs show clear variations according to the orientation of the magnetization between two $CrPS_4$ layers, we observed magnetic fields in which the magnetization of $CrPS_4$ flipped and realized infinite MR for the first time in vdW heterostructures. However, due to the numerous layers of $CrPS_4$ and structural problems in our devices, clear analysis of exchange splitting and suspected spin transport could not be performed successfully. Thus, further experiments are being planned by redesigning the $NbSe_2/CrPS_4$ devices with a modified layout, alternative material for electrodes and a few layers of $CrPS_4$. Because the flips in magnetization of $CrPS_4$ will be countable in this revised structure, it is expected that some unidentified effects, such as exchange splitting and spin transport, will be able to analyze.

In summary, we observed the magnetic proximity effect through broken superconductivity and infinite MR induced by exchange fields for the first time in an AFI/SC/AFI vdW heterostructure. Although there still exist curious results requiring further verification, based on the above findings, we suggest our $CrPS_4/NbSe_2$ vdW heterostructure as a new and potential platform for studying exchange fields between superconductors and ferromagnets.

Bibliography

1. Gennes, P. G. D. COUPLING BETWEEN FERROMAGNETS. *PHYSICS LETTERS* **23**, 2 (1966).
2. Strambini, E. *et al.* Revealing the magnetic proximity effect in EuS/Al bilayers through superconducting tunneling spectroscopy. *Phys. Rev. Materials* **1**, 054402 (2017).
3. Gu, J. Y. *et al.* Magnetization-Orientation Dependence of the Superconducting Transition Temperature in the Ferromagnet-Superconductor-Ferromagnet System: C u N i / N b / C u N i. *Phys. Rev. Lett.* **89**, 267001 (2002).
4. Potenza, A. & Marrows, C. H. Superconductor-ferromagnet CuNi / Nb / CuNi trilayers as superconducting spin-valve core structures. *Phys. Rev. B* **71**, 180503 (2005).
5. Moraru, I. C., Pratt, W. P. & Birge, N. O. Magnetization-Dependent T c Shift in Ferromagnet/Superconductor/Ferromagnet Trilayers with a Strong Ferromagnet. *Phys. Rev. Lett.* **96**, 037004 (2006).
6. Miao, G.-X., Yoon, K., Santos, T. S. & Moodera, J. S. Influence of Spin-Polarized Current on Superconductivity and the Realization of Large Magnetoresistance. *Phys. Rev. Lett.* **98**, 267001 (2007).
7. Li, B. *et al.* Superconducting Spin Switch with Infinite Magnetoresistance Induced by an Internal Exchange Field. *Phys. Rev.*

Lett. **110**, 097001 (2013).

8. Zhu, Y., Pal, A., Blamire, M. G. & Barber, Z. H. Superconducting exchange coupling between ferromagnets. *Nature Mater* **16**, 195–199 (2017).

9. Hao, X., Moodera, J. S. & Meservey, R. Spin-filter effect of ferromagnetic europium sulfide tunnel barriers. *Phys. Rev. B* **42**, 8235–8243 (1990).

10. Xiong, Y. M., Stadler, S., Adams, P. W. & Catelani, G. Spin-Resolved Tunneling Studies of the Exchange Field in EuS / Al Bilayers. *Phys. Rev. Lett.* **106**, 247001 (2011).

11. Wolf, M. J., Sürgers, C., Fischer, G. & Beckmann, D. Spin-polarized quasiparticle transport in exchange-split superconducting aluminum on europium sulfide. *Phys. Rev. B* **90**, 144509 (2014).

12. Linder, J. & Robinson, J. W. A. Superconducting spintronics. *Nature Phys* **11**, 307–315 (2015).

13. Ajayan, P., Kim, P. & Banerjee, K. Two-dimensional van der Waals materials. *Physics Today* **69**, 38–44 (2016).

14. Geim, A. K. & Grigorieva, I. V. Van der Waals heterostructures. *Nature* **499**, 419–425 (2013).

15. Liu, Y. *et al.* Van der Waals heterostructures and devices. *Nat Rev Mater* **1**, 16042 (2016).

16. Lu, J. M. *et al.* Evidence for two-dimensional Ising superconductivity in gated MoS2. *Science* **350**, 1353–1357 (2015).

17. Saito, Y. *et al.* Superconductivity protected by spin-valley locking in ion-gated MoS2. *Nature Phys* **12**, 144–149 (2016).

18. de la Barrera, S. C. *et al.* Tuning Ising superconductivity with layer and spin-orbit coupling in two-dimensional transition-metal dichalcogenides. *Nat Commun* **9**, 1427 (2018).

19. Hsu, Y.-T., Vaezi, A., Fischer, M. H. & Kim, E.-A. Topological superconductivity in monolayer transition metal dichalcogenides. *Nat Commun* **8**, 14985 (2017).

20. Xi, X. *et al.* Ising pairing in superconducting NbSe2 atomic layers. *Nature Phys* **12**, 139–143 (2016).

21. Tsen, A. W. *et al.* Nature of the quantum metal in a two-dimensional crystalline superconductor. *Nature Phys* **12**, 208–212 (2016).

22. Khestanova, E. *et al.* Unusual Suppression of the Superconducting Energy Gap and Critical Temperature in Atomically Thin $NbSe_2$. *Nano Lett.* **18**, 2623–2629 (2018).

23. Zhuang, H. L., Kent, P. R. C. & Hennig, R. G. Strong anisotropy and magnetostriction in the two-dimensional Stoner ferromagnet Fe 3 GeTe 2. *Phys. Rev. B* **93**, 134407 (2016).

24. Gibertini, M., Koperski, M., Morpurgo, A. F. & Novoselov, K. S. Magnetic 2D materials and heterostructures. *Nat. Nanotechnol.* **14**, 408–419 (2019).

25. Lee, J. *et al.* Structural and Optical Properties of Single- and

Few-Layer Magnetic Semiconductor $CrPS_4$. *ACS Nano* **11**, 10935–10944 (2017).

26. Alicea, J. Majorana fermions in a tunable semiconductor device. *Phys. Rev. B* **81**, 125318 (2010).

27. Moodera, J. S., Miao, G.-X. & Santos, T. S. Frontiers in spin-polarized tunneling. *Physics Today* **63**, 46–51 (2010).

28. Quay, C. H. L., Chevallier, D., Bena, C. & Aprili, M. Spin imbalance and spin-charge separation in a mesoscopic superconductor. *Nature Phys* **9**, 84–88 (2013).

29. Banerjee, S. S. *et al.* Magnetic phase diagram of anisotropic superconductor 2H-NbSe2. *Physica B: Condensed Matter* **237–238**, 315–317 (1997).

30. Falk, A. *et al.* Magnetic switching of phase-slip dissipation in NbSe 2 nanoribbons. *Phys. Rev. B* **75**, 020501 (2007).

31. Srivastava, P. K. *et al.* Exchange Bias Effect in Ferro-/Antiferromagnetic van der Waals Heterostructures. *Nano Lett.* **20**, 3978–3985 (2020).

32. Huang, B. *et al.* Electrical control of 2D magnetism in bilayer CrI3. *Nature Nanotech* **13**, 544–548 (2018).

33. Leksin, P. V. *et al.* Manifestation of New Interference Effects in a Superconductor-Ferromagnet Spin Valve. *Phys. Rev. Lett.* **106**, 067005 (2011).

34. Zhong, D. *et al.* Van der Waals engineering of ferromagnetic

semiconductor heterostructures for spin and valleytronics. *Sci. Adv.* **3**, e1603113 (2017).

35. Kim, M. *et al.* Strong Proximity Josephson Coupling in Vertically Stacked $NbSe_2$–Graphene–$NbSe_2$ van der Waals Junctions. *Nano Lett.* **17**, 6125–6130 (2017).

36. Hirsch, J. E. Spin Hall Effect. *Phys. Rev. Lett.* **83**, 1834–1837 (1999).

37. Saitoh, E., Ueda, M., Miyajima, H. & Tatara, G. Conversion of spin current into charge current at room temperature: Inverse spin-Hall effect. *Appl. Phys. Lett.* **88**, 182509 (2006).

38. Liu, L., Moriyama, T., Ralph, D. C. & Buhrman, R. A. Spin-Torque Ferromagnetic Resonance Induced by the Spin Hall Effect. *Phys. Rev. Lett.* **106**, 036601 (2011).

39. Liu, L., Lee, O. J., Gudmundsen, T. J., Ralph, D. C. & Buhrman, R. A. Current-Induced Switching of Perpendicularly Magnetized Magnetic Layers Using Spin Torque from the Spin Hall Effect. *Phys. Rev. Lett.* **109**, 096602 (2012).

40. Nakayama, H. *et al.* Spin Hall Magnetoresistance Induced by a Nonequilibrium Proximity Effect. *Phys. Rev. Lett.* **110**, 206601 (2013).

41. Borisenko, S. V. *et al.* Two Energy Gaps and Fermi-Surface "Arcs" in NbSe 2. *Phys. Rev. Lett.* **102**, 166402 (2009).

42. Flicker, F. & van Wezel, J. Charge order from orbital-dependent

coupling evidenced by NbSe2. *Nat Commun* **6**, 7034 (2015).

43. Koley, S., Mohanta, N. & Taraphder, A. The unusual normal state and charge-density-wave order in 2H-$NbSe_2$. *J. Phys.: Condens. Matter* **27**, 185601 (2015).

44. Bawden, L. *et al.* Spin–valley locking in the normal state of a transition-metal dichalcogenide superconductor. *Nat Commun* **7**, 11711 (2016).

45. Nakata, Y. *et al.* Anisotropic band splitting in monolayer NbSe2: implications for superconductivity and charge density wave. *npj 2D Mater Appl* **2**, 12 (2018).

46. Andronov, A., Gordion, I., Kurin, V., Nefedov, I. & Shereshevsky, I. Kinematic vortices and phase slip lines in the dynamics of the resistive state of narrow superconductive thin film channels. *Physica C: Superconductivity and its Applications* **213**, 193–199 (1993).

47. Berdiyorov, G. R., Elmurodov, A. K., Peeters, F. M. & Vodolazov, D. Y. Finite-size effect on the resistive state in a mesoscopic type-II superconducting stripe. *Phys. Rev. B* **79**, 174506 (2009).

48. Berdiyorov, G. *et al.* Dynamics of current-driven phase-slip centers in superconducting strips. *Phys. Rev. B* **90**, 054506 (2014).

49. Paradiso, N., Nguyen, A.-T., Enzo Kloss, K. & Strunk, C. Phase slip lines in superconducting few-layer $NbSe_2$ crystals. *2D Mater.* **6**, 025039 (2019).

국 문 요 약

초전도체(SC)와 강자성체(FM)의 접합에서, 초전도 상태는 강자성체로 인한 Exchange field로 인해 조절될 수 있다. Exchange field가 강해질수록 초전도 상태가 약해지는 성질을 이용하여 FM/SC/FM 구조에서 두 자성체의 상대적 자화 방향에 따른 초전도 전이 온도의 조절, 무한대의 자기저항이 실험적으로 보고되었으며, 최근에는 EuS/Al 구조에서 외부 자기장이 가해지지 않은 상태에서도 초전도 갭 부근에서 스핀 방향에 따른 에너지 레벨의 분리 또한 실현되었다. 그러나 기존 연구는 모두 다결정 나노 필름 형태의 구조에서 실험이 진행되어 왔으며, 원자단위로 평평하고 결함이 최소화된 2차원 반데르발스 물질에서의 연구는 아직 진행된 바 없다. 이런 장점을 활용, 2차원 반데르발스 초전도체 $NbSe_2$와 반강자성체 $CrPS_4$를 사용하여 단결정 수준에서 연구를 진행하였다. $CrPS_4/NbSe_2/CrPS_4$ 구조에서 $CrPS_4$의 Exchange field에 의해 $NbSe_2$층의 초전도 상태가 깨질 수 있음을 확인하였고, $NbSe_2$에 인접한 위층과 아래층 $CrPS_4$의 자화 방향이 평행/반평행한 경우에 따라 $NbSe_2$의 비소산성(Non-dissipative) 전류 수송이 유지되는 영역이 실제 측정이 가능한 수준으로 확연하게 달라짐을 확인함으로써 무한대의 자기저항을 측정하였다. 또한, 소자 구조상의 문제로 확실한 분석이 불가능했던 스핀 수송, 스핀 방향에 따른 에너지 레벨의 분리에 대한

검증을 위하여 기존 소자가 갖는 문제점을 개선한 새로운 소자를 디자인하여 현재 추가 실험을 계획 중에 있다. 비록 아직 추가 실험과 분석이 필요한 단계이지만, 원자층 단위로 조절이 가능한 2차원 반데르발스 구조에서는 최초로 초전도체와 자성체 사이의 명확한 자기 근접 효과를 확인하였기에, $CrPS_4$와 $NbSe_2$의 반데르발스 이종접합 구조가 Exchange field 연구를 위한 새롭고 잠재력 높은 플랫폼이 될 수 있음을 제시하였다.

Keywords: 2D superconductor, 2D antiferromagnetic insulator, van der Waals heterostructure, Electric transport measurement, Niobium diselenide, Chromium thiophosphate.

Student Number: 2018-28679